Journal of Power Sources 226 (2013) 173–178

Contents lists available at SciVerse ScienceDirect

Journal of Power Sources

journal homepage: www.elsevier.com/locate/jpowsour

Photovoltaic performance degradation and recovery of the flexible dye-sensitized solar cells by bending and relaxing

Xue-Long He [a], Mei Liu [a], Guan-Jun Yang [a,*], Hai-Long Yao [a], Sheng-Qiang Fan [b], Chang-Jiu Li [a,*]

[a] State Key Laboratory for Mechanical Behavior of Materials, School of Materials Science and Engineering, Xi'an Jiaotong University, Xi'an, Shaanxi 710049, PR China
[b] Center for Organic Photonics & Electronics, School of Chemistry & Molecular Biosciences, The University of Queensland, QLD 4072, Australia

HIGHLIGHTS

- Photovoltaic performance of flexible DSCs under bending was first reported.
- Photovoltaic performance degradation and recovery mechanism was investigated.
- A modified equivalent circuit model for DSCs under bending state was proposed.

ARTICLE INFO

Article history:
Received 8 June 2012
Received in revised form
26 August 2012
Accepted 17 October 2012
Available online 26 October 2012

Keywords:
Dye-sensitized solar cells
Photovoltaic performance
Short circuit
Titanium dioxide film
Electrochemical impedance spectroscopy

ABSTRACT

Flexibility, as well as high efficiency, of flexible dye-sensitized solar cells (DSCs) is of significant importance to their application. In this study, the photovoltaic performance of the flexible DSCs under bending and relaxed states is investigated to understand the degradation and recovery of the photovoltaic performance. Results show that when the bending radius is larger than 8 mm, the photovoltaic parameters of the flexible DSCs maintain the same values as those in the relaxed states. However, when the bending radius is reduced to 8 mm, the photovoltaic performance is two orders of magnitude decreased. Most interestingly, when the bending DSCs are relaxed, the photovoltaic performance is found to be completely recovered. The microstructure observation shows that the direct contact between TiO_2 film and counter electrode (CE) occurred at the bending radius of 8 mm, which should be the main reason for their low photovoltaic performance in the bending state. Finally, a modified equivalent circuit model is proposed for the flexible DSCs under bending condition.

1. Introduction

Dye-sensitized solar cells (DSCs) have currently attracted widespread academic and commercial interests as a next generation photovoltaic device due to their relatively high energy conversion efficiency and low production cost [1]. Recently, there is an increasing interest in replacing rigid glass substrates with plastic substrates in considerations of light weight, flexibility and compatibility with low-cost roll-to-roll production [2–4].

Generally, high-temperature sintering (~450 °C) is required to construct the strong connection between nanoparticles and thereby the rapid electron diffusion in the photoanode for the conventional DSCs on conductive glass substrates [5]. However, the high temperature treatment cannot be employed on the conductive plastic substrates due to the low heat-resistance temperature (about 150 °C) of the plastic materials [6]. In order to improve the nanoparticle connection and mechanical stability of the TiO_2 films on such plastic substrates, other methods which can be performed at low temperature are thus expected. Over the last few years, a couple of effective methods which have been developed for plastic photoanodes include mechanical compression [7], microwave irradiation [8], hydrothermal crystallization [9], chemical sintering [10], electron-beam annealing [11], electrophoretic deposition [12] and room temperature cold spraying [13,14].

Up to now, the highest energy conversion efficiency of the assembled plastic DSCs has been up to 8.1%, which is nearly 70% of the conventional glass-based DSCs [15]. However, the flexibility, one of the most important parameters of the plastic DSCs, is rarely reported so far. Most work has been focused on improving the mechanical stability of the plastic photoanode under bending state. As an example, Jiang et al. [16] used nanowire to replace nanoparticle in the preparation of photoanode for flexible DSCs, which demonstrated a high flexibility. Li et al. [17] also improved the

* Corresponding authors. Tel.: +86 29 82665299; fax: +86 29 82660970.
E-mail addresses: ygj@mail.xjtu.edu.cn (G.-J. Yang), licj@mail.xjtu.edu.cn (C.-J. Li).

0378-7753/$ – see front matter © 2012 Elsevier B.V. All rights reserved.
http://dx.doi.org/10.1016/j.jpowsour.2012.10.056

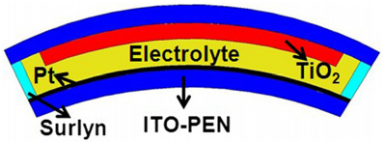

Fig. 1. The schematic of the flexible DSCs under outward bending.

flexibility by blending elastic polymer PMMA with TiO_2, though the efficiency was decreased by the presence of polymer in TiO_2 film. For all the studies until now, it should be noted that the reported photovoltaic performance of the flexible DSC was obtained for the DSCs at relaxed state. Since the flexible DSCs may work at both bending and relaxed states, the cell performance under bending state is likewise important.

In this study, TiO_2 films were fabricated on the plastic substrates by using room temperature cold spray method. The cell performance of the assembled plastic DSCs under both bending and relaxed states was investigated to examine the evolution of cell performance during bending and relaxing. The relationship between photovoltaic performance, electrochemical properties and microstructure of TiO_2 film in the flexible DSCs was studied to aim at understanding the factors which dominates the performance of flexible DSCs.

2. Experimental

2.1. Fabrication of TiO_2 film and flexible DSCs

The TiO_2 film was prepared by a home-developed room temperature cold spray system [13,14,18] using a commercial TiO_2 powder (P25, Degussa, 70% anatase and 30% rutile) with a thickness of 10 μm on ITO-PEN plastic substrate (PECF-IP, 15 Ω sq^{-1}, Peccell). The electrode was heated at 135 °C for 15 min. After cooled to 80 °C, the photoanode was immersed in an absolute ethanol solution containing 0.3 mM N719 dye (Solaronix) for 24 h, then rinsed with absolute ethanol and dried with nitrogen gas. The photoanode was then used to assemble DSCs with a plastic Pt counter electrode (CE) using a 60 μm thick Surlyn film (1702, DuPont) spacer. The electrolyte solution was introduced into the cell through four holes predrilled on the back of the plastic CE, then the holes were sealed up using an UV resin (ThreeBond). The electrolyte solution was composed of 0.6 M DMPII (Institute of Plasma Physics), 0.05 M I_2 (Aldrich), 0.1 M LiI (Aldrich), and 0.5 M 4-*tert*-butylpyridine (Acros) in dehydrated acetonitrile (Aldrich).

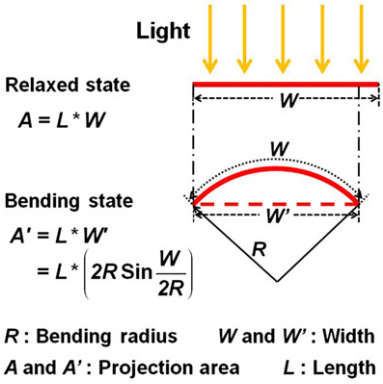

Fig. 2. The schematic of the calculation of the projection area of the photoanode under bending state and relaxed state.

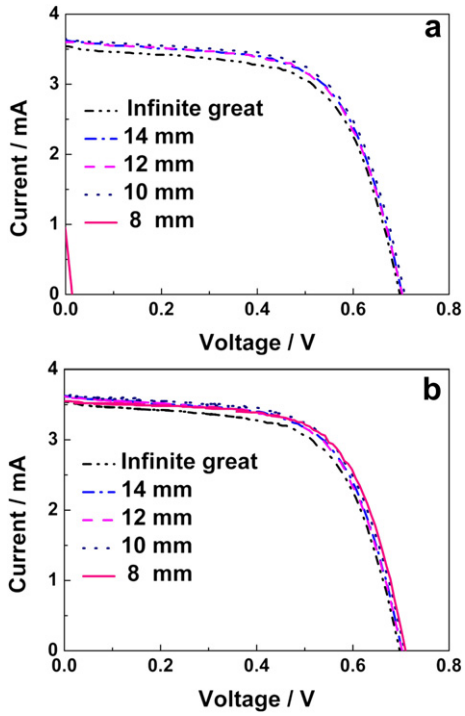

Fig. 3. The I–V curves of the flexible DSCs measured under bending state (a) and relaxed state (b) with different bending radii.

2.2. Characterization of flexible DSCs

The bending test was carried out by a home-developed flexible solar cell bending tester, by which the bending conditions, including bending direction, bending radius and bending times, were accurately controlled. Fig. 1 shows the schematic of the flexible DSC under outward bending. The photovoltaic performance of

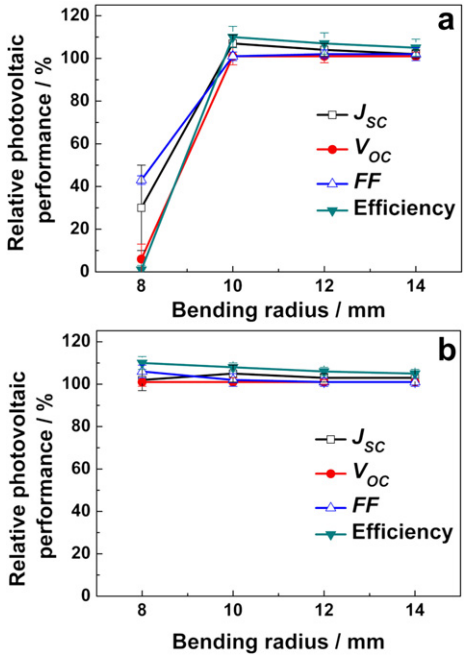

Fig. 4. Relative photovoltaic parameters of the flexible DSCs measured under bending state (a) and relaxed state (b) as a function of bending radius.

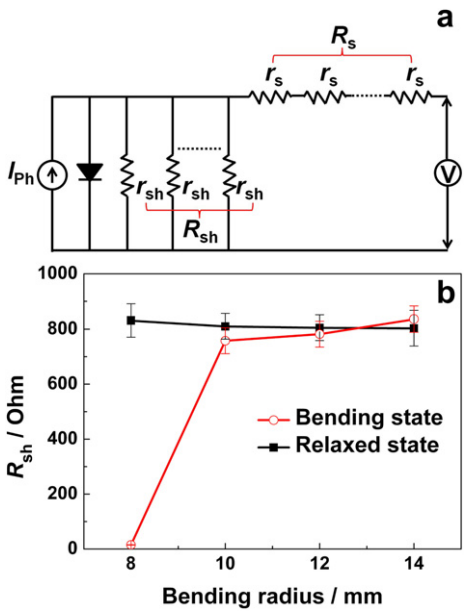

Fig. 5. Diode-model for flexible DSCs (a), relationship between the parallel resistance R_{sh} of the flexible DSCs under bending and relaxed states with different bending radii (b).

flexible DSCs under different conditions was measured using a solar simulator (100 mW cm^{-2}, Oriel 94023A, Newport) equipped with a Keithley 2400 digital source meter. The active area of the cells was controlled to be 0.48 cm^2. The active area herein is referred to as the area of the photoanode. The width (W) and length (L) of the photoanode were 6 mm and 8 mm, respectively.

The photo-to-electric energy conversion efficiency (η) of the flexible DSC under relaxed state and bending state is calculated using the following formula:

$$\eta = \frac{P_{EMax}}{P_I} = \frac{I_{Max} \times V_{Max}}{D \times A} \quad (1)$$

where P_{EMax} is the maximum power of the solar cell, P_I is the light power obtained by the photoanode, I_{Max} and V_{Max} is the current and the voltage at the maximum electric power of the solar cell, D is the light power density, and A is the projection area of the photoanode in the light illumination direction. Fig. 2 shows the schematic of the calculation of the projection area of the photoanode under bending state and relaxed state.

The electrochemical properties of the flexible DSCs were investigated by electrochemical impedance spectroscopy (EIS). The EIS spectra were measured in the dark at −0.7 V bias potential using a CHI606 electrochemical workstation (Shanghai Chenhua Instrument). The spectra were scanned in a frequency ranging from 10^{-1}–10^5 Hz with an ac amplitude of 10 mV. The obtained impedance spectra were fitted with the Z-view software in terms of appropriate equivalent circuit model. In order to examine the effect of bending tests on the structure of both photoanode and Pt counter electrode, they were detached from the tested DSCs, rinsed with acetonitrile and ethanol sequentially for removal of the electrolyte, and then observed by a field emission scanning electron microscope (FESEM, QUANTA 600F).

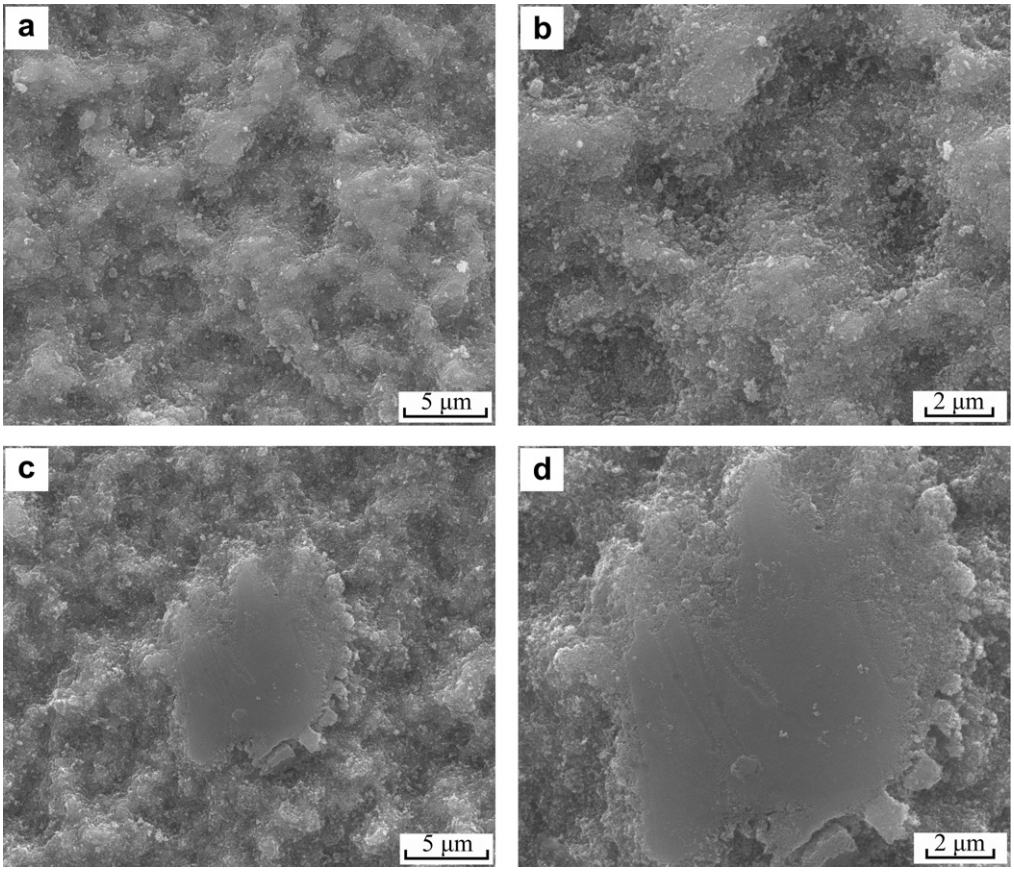

Fig. 6. Surface morphologies of the photoanodes under relaxed state without (a, b) and with (c, d) bending at a radius of 8 mm.

3. Results and discussion

3.1. Photovoltaic performance of the flexible DSCs under single outward bending

Before the bending test, the photovoltaic parameters of the assembled flexible DSCs were measured. The short-circuit photocurrent density (J_{SC}) is 7.21 mA cm^{-2}, the open-circuit photovoltage (V_{OC}) is 0.63 V, the fill factor (*FF*) is 0.61, and the energy conversion efficiency is 2.78%. Fig. 3 shows the I–V curves of the flexible DSCs under bending state and relaxed state with different bending radii. Fig. 4 shows the relative photovoltaic parameters of the flexible DSCs as a function of bending radius measured under bending state and relaxed state. As for the photovoltaic performance measured under bending state (Fig. 4a), the cell performance is not significantly influenced when the bending radius is larger than 8 mm, suggesting an excellent mechanical stability of the TiO_2 films prepared by room temperature cold spray method. However, when the bending radius is decreased to 8 mm, a sharp decrease of the photovoltaic performance is observed. Most interestingly, when the flexible DSCs are relaxed, the cell performance completely recovers as shown in Fig. 4b.

There are two possible pathways for the DSCs losing their photovoltaic performance under very small-radius bending state. Firstly, the TiO_2 film is under tension when the cell is under outward bending as shown in Fig. 1. Since the TiO_2 film is fragile and may crack and peel off under tension, the degradation of the cell performance is probably caused by the crack of the TiO_2 film. However, due to the fact that the photovoltaic performance can be fully recovered when the bent cell goes back to the relaxed state, the crack of the TiO_2 films may not be the main reason resulting in the degradation of the cell performance. Secondly, under bending state the TiO_2 film may directly contact with the Pt CE, thus leading to short circuit. In order to clarify this issue, the parallel resistance R_{sh} of the flexible DSCs is calculated according to the diode model shown in Fig. 5a. The results are shown in Fig. 5b. As can be seen, the variation of R_{sh} as a function of the bending radius displays the same tendency with the corresponding photovoltaic performance as shown in Fig. 4a. The R_{sh} maintains the same when the bending radius is larger than 8 mm. When the bending radius is reduced to 8 mm, a significant decrease from 822 Ω to 15 Ω is observed. The low R_{sh} means a very small parallel resistance is produced in the electrical circuit as shown in Fig. 3a, reflecting the assumption of short circuit occurring. As expected, after the DSC is relaxed from bending, the R_{sh} recovers to 831 Ω, which is comparable to its original value. In addition, the electrolyte leak is not found before and after DSC bending. Therefore, all the facts here have pointed out the reversibility of photovoltaic performance of such flexible DSCs.

3.2. Surface morphologies of the electrodes in the flexible DSCs after single outward bending

Since the photovoltaic performance of the flexible DSCs significantly changed by relaxing and bending, the defects on both photoanodes and CEs may be formed after bending and relaxing cycles. Investigations on this issue have been performed by morphology characterization using FESEM under relaxed state after bending process. No peeling off was observed on both photoanodes and CEs. Fig. 6 shows the surface morphologies of the photoanodes without and with bending at a radius of 8 mm. As can be seen from Fig. 6a and b, the as-prepared primary TiO_2 photoanode presents a rough morphology. However, after bending with a radius of 8 mm, part of the surface demonstrates flat surface, perhaps due to the squeezing effect by the Pt CE as shown in Fig. 6c and d. Furthermore, the surface morphologies of the Pt CEs are also characterized and shown in Fig. 7. Compared to the surface morphology of the Pt

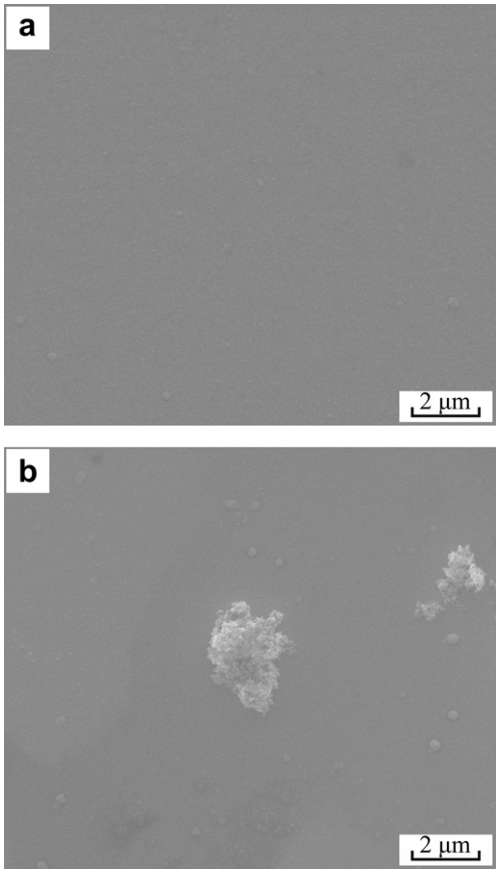

Fig. 7. Surface morphologies of the Pt CEs under relaxed state without (a) and with (b) bending at a radius of 8 mm.

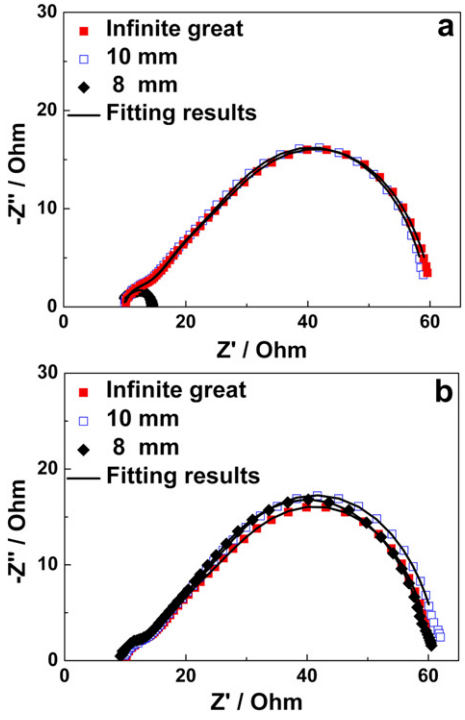

Fig. 8. Nyquist plots of the flexible DSCs under bending state (a) and relaxed state (b) after experiencing the bending process with different bending radii.

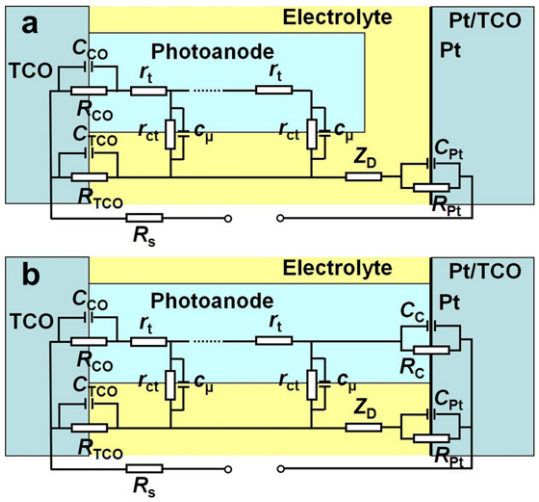

Fig. 9. Generalized equivalent circuit model for a complete DSC (a), where R_s is the series resistance, R_{CO} and C_{CO} are the resistance and the capacitance at the TCO/TiO_2 interface, R_{TCO} and C_{TCO} are the resistance and the capacitance at the exposed TCO/electrolyte interface, R_t ($=r_t \cdot L$) is the transport resistance of the electrons in the TiO_2 film, R_{ct} ($=r_{ct} \cdot L$) is the charge transfer resistance of electrons at the TiO_2/dye/electrolyte interface, C_μ ($=c_\mu \cdot L$) is the chemical capacitance of TiO_2 film, Z_D is the Nernst diffusion resistance of the electrolyte, R_{Pt} and C_{Pt} are the charge transfer resistance and electrical double layer capacitance at the Pt/electrolyte interface, L is the thickness of the TiO_2 film. Modified equivalent circuit model for an internal short circuit DSC (b), where C_C and R_C are the resistance and the capacitance of the contacted TiO_2/Pt/TCO interface.

CE without bending at 8 mm (Fig. 7a), it is obviously observed that there are some TiO_2 nanoparticles appearing on the Pt CE with bending at a radius of 8 mm (Fig. 7b). This is evident to support our consumption on the short circuit between the photoanode and CE under bending with a radius of 8 mm. In brief, the internal short circuit of the photoanode and CE is the main reason responsible for the serious loss of the photovoltaic performance of the flexible DSCs.

3.3. Electrochemical properties of the flexible DSCs under single outward bending

Equivalent circuit has been employed to correlate the photovoltaic performance and electrochemical properties of the DSCs, which has helped the deep understanding on the DSC structure–performance relationship. The typical Nyquist plots are displayed in Fig. 8. Two arcs are distinguished in the frequency range of 10^3–10^5 Hz and 10^{-1}–10^3 Hz, from left to right. These arcs can be assigned to the transport process of the electrons at the interface of Pt/electrolyte and TiO_2/dye/electrolyte, respectively. A generalized equivalent circuit model [19–21] shown in Fig. 9a was employed to fit the EIS data using a Z-view software. The electrochemical properties are listed in Table 1. However, the state-of-the-art equivalent circuit (Fig. 9a) is insufficient to model the DSCs under deeply-bent state due to the direct contact of the photoanode with CE.

Table 1
The electrochemical properties of the flexible DSCs under bending and relaxed states with different bending radii fitted by generalized equivalent circuit model and modified equivalent circuit model.

Bending radius	Measurement condition	R_s/Ω	R_t/Ω	R_{ct}/Ω	R_s^*/Ω	R_t^*/Ω	R_{ct}^*/Ω	R_c^*/Ω
Infinite great	–	9.3	45.5	33.8	9.9	45.1	34.1	8.8×10^{20}
10 mm	Bending state	9.3	40.9	34.7	9.8	40.8	34.9	1.2×10^{19}
8 mm	Bending state	–	–	–	7.8	6.6	3.3	3.7
10 mm	Relaxed state	9.2	37.7	38.2	9.7	37.8	38.3	8.0×10^{19}
8 mm	Relaxed state	8.6	33.5	38.1	9.1	33.6	38.2	1.0×10^{20}

*Refers to the data obtained by using the modified equivalent circuit model.

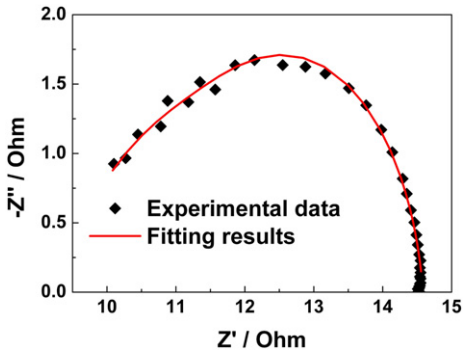

Fig. 10. Nyquist plots and fitting results of the flexible DSCs under bending state with a radius of 8 mm using the modified equivalent circuit model shown in Fig. 9b.

At this point, a brief note should be made about the EIS measuring mechanism of the DSC in the dark. In the dark, the DSC behaves as a leaking capacitor [21]. When applying forward bias, the electrons are injected from the TCO substrate and transported through the mesoporous TiO_2 network. Meanwhile, the electrons react with I_3^- ions in the electrolyte. I_3^- ions are generated at CE and penetrates the mesoporous TiO_2 films by diffusion [22,23]. However, if the photoanode contacts with the CE, the injected electrons can transport to the CE directly. Considering this, a modified equivalent circuit model for the internal short circuit DSCs is proposed as shown in Fig. 9b, where the R_C and C_C are the resistance and capacitance of the contacted TiO_2/Pt interface.

After using the modified equivalent circuit model, a perfect fitting results of the flexible DSCs bent at 8 mm is obtained as shown in Fig. 10. Besides, the model can be also used to fit the EIS data obtained for flexible DSCs under other measuring conditions. The fitting results using the modified equivalent circuit model (Fig. 9b) only varied by less than ±5% upon replacement of the generalized equivalent circuit model (Fig. 9a) as shown in Table 1.

As listed in Table 1, the R_c value is 3.7 Ω for the flexible DSCs bent at 8 mm, which is several orders of magnitude smaller than that of the flexible DSCs under other measuring conditions. This is also a direct proof for the internal short circuit of the flexible DSC bent at 8 mm. Furthermore, when the bending radius is 8 mm, the R_t and R_{ct} are significantly decreased. This is because that when the DSC is in internal short circuit state, the electrons can rapidly transport to the CE, resulting in a much increased electron density which is beneficial to obtain a lower R_t and R_{ct}. Likewise, when the flexible DSCs relaxes, the R_t and R_{ct} values recover. Therefore, the modified equivalent circuit model proposed in this study can be used to fit the EIS data for flexible DSCs in all cases. By using this modified model, not only the internal short circuit phenomenon can be explored, but also the contact between photoanode and CE can be quantitatively detected. This will provide detailed information for understanding the evolution of photovoltaic performance of flexible solar cells under bending condition.

4. Conclusions

The photovoltaic performance of the flexible DSCs under bending state and relaxed state was measured. The photovoltaic performance was not significantly influenced when the bending radius was larger than 8 mm, showing an excellent mechanical stability of the TiO_2 films prepared by room temperature cold spray

method. When the bending radius was reduced to 8 mm, the photovoltaic performance was two orders of magnitude decreased. However, when the flexible DSC was relaxed, the cell performance was completely recovered. The microstructure results showed that when the DSC was bent at 8 mm, the direct contact between TiO_2 film of photoanode and CE occurred based on both the squeezed flat surface morphology of the TiO_2 film and the attachment of TiO_2 particles onto CE surface. As a result, the dramatically degradation of cell performance is mainly attributed to the internal short circuit between the photoanode and CE. Besides, a modified equivalent circuit model was proposed to characterize the electrochemical properties of the flexible DSCs under bending conditions.

Acknowledgments

The work was supported by the National Science Foundation of China (No.: 51072160, 50725101), Program for New Century Excellent Talents in University (No. NCET-08-0443), Program for Young Excellent Talents in Shaanxi Province (No. 20kjxx32), and the Fundamental Research Funds for the Central Universities.

References

[1] B. Oregan, M. Gratzel, Nature 353 (1991) 737–740.
[2] H.C. Weerasinghe, P.M. Sirimanne, G.P. Simon, Y.B. Cheng, J. Photochem. Photobiol. A Chem. 206 (2009) 64–70.
[3] M. Toivola, J. Halme, K. Miettunen, K. Aitola, P.D. Lund, Int. J. Energy Res. 33 (2009) 1145–1160.
[4] X.L. He, M. Liu, G.J. Yang, S.Q. Fan, C.J. Li, Appl. Surf. Sci. 258 (2011) 1377–1384.
[5] M.K. Nazeeruddin, A. Kay, I. Rodicio, R. Humphrybaker, E. Muller, P. Liska, N. Vlachopoulos, M. Gratzel, J. Am. Chem. Soc. 115 (1993) 6382–6390.
[6] Y. Kijitori, M. Ikegami, T. Miyasaka, Chem. Lett. 36 (2007) 190–191.
[7] H. Lindstrom, A. Holmberg, E. Magnusson, S.E. Lindquist, L. Malmqvist, A. Hagfeldt, Nano Lett. 1 (2001) 97–100.
[8] D. Gutierrez-Tauste, I. Zumeta, E. Vigil, M.A. Hernandez-Fenollosa, X. Domenech, J.A. Ayllon, J. Photochem. Photobiol. A Chem. 175 (2005) 165–171.
[9] D.S. Zhang, T. Yoshida, K. Furuta, H. Minoura, J. Photochem. Photobiol. A Chem. 164 (2004) 159–166.
[10] N.G. Park, K.M. Kim, M.G. Kang, K.S. Ryu, S.H. Chang, Y.J. Shin, Adv. Mater. 17 (2005) 2349–2353.
[11] T. Kado, M. Yamaguchi, Y. Yamada, S. Hayase, Chem. Lett. 32 (2003) 1056–1057.
[12] W.H. Chiu, K.M. Lee, W.F. Hsieh, J. Power Sources 196 (2011) 3683–3687.
[13] S.Q. Fan, C.J. Li, C.X. Li, G.J. Liu, G.J. Yang, L.Z. Zhang, Mater. Trans. 47 (2006) 1703–1709.
[14] S.Q. Fan, C.J. Li, G.J. Yang, L.Z. Zhang, J.C. Gao, Y.X. Xi, J. Therm. Spray Technol. 16 (2007) 893–897.
[15] T. Yamaguchi, N. Tobe, D. Matsumoto, T. Nagai, H. Arakawa, Sol. Energy Mater. Solar Cells 94 (2010) 812–816.
[16] C.Y. Jiang, X.W. Sun, K.W. Tan, G.Q. Lo, A.K.K. Kyaw, D.L. Kwong, Appl. Phys. Lett. 92 (2008) 143101.
[17] Y. Li, K. Yoo, D.K. Lee, J.H. Kim, N.G. Park, K. Kim, M.J. Ko, Curr. Appl. Phys. 10 (2010) E171–E175.
[18] X.L. He, G.J. Yang, H.L. Yao, C.J. Li, S. Li, M. Li, S.Q. Fan, Rare Metal Mat. Eng. 41 (2012).
[19] F. Fabregat-Santiago, J. Bisquert, E. Palomares, L. Otero, D.B. Kuang, S.M. Zakeeruddin, M. Gratzel, J. Phys. Chem. C 111 (2007) 6550–6560.
[20] F. Fabregat-Santiago, J. Bisquert, G. Garcia-Belmonte, G. Boschloo, A. Hagfeldt, Sol. Energy Mater. Sol. Cells 87 (2005) 117–131.
[21] J. Bisquert, J. Phys. Chem. B 106 (2002) 325–333.
[22] Q. Wang, S. Ito, M. Gratzel, F. Fabregat-Santiago, I. Mora-Sero, J. Bisquert, T. Bessho, H. Imai, J. Phys. Chem. B 110 (2006) 25210–25221.
[23] Q. Wang, J.E. Moser, M. Gratzel, J. Phys. Chem. B 109 (2005) 14945–14953.